Coincidence Planar Imaging for Dynamic [^{18}F]FDG Uptake in Nude Mice with Tumors and Inflammation: Correlated with Histopathology and Micro-autoradiography

Ying-Ling Sun, Meei-Ling Jan, Pan-Fu Kao,[1] Kuo-Hsien Fan, Hui-Ting Hsu,[1] Wen-Chen Chang,[2] Young-Chi Shen,[2] and Te-Wei Lee

Institute of Nuclear Energy Research, Lung-Tan, [1]Department of Nuclear Medicine, Buddhist Xindian Tzu Chi General Hospital and Tzu Chi College of Technology, and [2]Department of Medical Oncology, Chang-Gung Memorial Hospital, Taipei, Taiwan.

The Institute of Nuclear Energy Research of Taiwan has developed a dynamic coincidence detection device for positron emitted radiotracer pharmacodynamic study in small mice models. In this study, we set up an experimental paradigm by determining [fluorine-18]-2-deoxy-2-fluoro-D-glucose ([^{18}F]FDG) dynamic uptake in tumors and inflammations in nude mice as the foundation for future applications in therapy development. Histopathology and micro-autoradiography of these tumors and inflammations were obtained for confirmation. Dynamic coincidence planar images of six tumors and two inflammations in nude mice were acquired over 4 hours immediately after injection of 25.9 MBq of [^{18}F]FDG into the right thigh of each animal. After image reconstruction, the lesion-to-background ratios were calculated in regions of interest over the lesion and contralateral thigh to determine the equilibrium status of the radiotracer. All mice were sacrificed for histopathologic examination and six of the mice were examined with micro-autoradiography. [^{18}F]FDG uptake in tumors and inflammations both reached equilibrium about 3 hours after injection. At equilibrium, [^{18}F]FDG uptake into tumors was two to four times higher than the background. Uptake into the 4-day and 8-day inflammations was 2.3 and 5.5 times higher than the background, respectively. Histopathology showed macrophage and neutrophil infiltration around the tumors and in the inflammations. Micro-autoradiography showed dense silver grains in the granulation tissue surrounding the tumors and inflammations. The preliminary results suggested that dynamic [^{18}F]FDG coincidence planar imaging can help in determining the suitable time for static [^{18}F]FDG imaging in nude mice models. The optimal time for static [^{18}F]FDG positron emission tomography imaging was around 3 hours after injection. The paradigm for determining a dynamic [^{18}F]FDG uptake pattern was demonstrated for future new therapeutic drug experimental use.

Key Words: [fluorine-18]-2-deoxy-2-fluoro-D-glucose, nude mice, dynamic coincidence planar image

(*Kaohsiung J Med Sci* 2005;21:258–66)

Diagnosing and monitoring diseases using less invasive, more sophisticated imaging modalities, such as positron emission tomography (PET), is becoming increasingly common. PET imaging technology uses compounds labeled with positron-emitting radioisotopes to visualize and measure molecular processes [1]. Molecular imaging with PET is sensitive and informative to biologic processes of diseases [2].

[Fluorine-18]-2-deoxy-2-fluoro-D-glucose ([^{18}F]FDG) is a radiotracer that is useful for the PET imaging of glucose

Received: February 4, 2005 Accepted: April 12, 2005
Address correspondence and reprint requests to: Dr. Pan-Fu Kao, Department of Nuclear Medicine, Buddhist Xindian Tzu Chi General Hospital, 289 Jian Guo Road, Xindian, Taipei 231, Taiwan
E-mail: kaopanfu@tzuchi.org.tw

metabolism. Unlike glucose-6-phosphate, [18F]FDG-6-phosphate cannot undergo further metabolism after phosphorylation and becomes trapped in the cell [3]. For years, scientists have known that cancer cells undergo accelerated glycolysis [4]. The high uptake of [18F]FDG into tumor cells is due to a characteristic phenotype of malignant metabolism that leads to an increase in glycolysis [5]. Therefore, each cancer cell seems to have a characteristic rate of glucose metabolism [6].

[18F]FDG PET scans are cost-effective for cancer staging and detecting recurrence or distant metastases in lymphoma, melanoma, colorectal, lung, and esophageal cancers, and cancer of the head and neck [7]. Recent investigations, however, have demonstrated that inflammatory cells such as macrophages and neutrophils also use increased amounts of glucose during chemotaxis and phagocytosis, which can be clearly visualized *in vivo* at the site of inflammation and infection [8]. Consequently, [18F]FDG accumulates not only in malignant tumors but also inflammations. Zhuang et al reported that dual time point [18F]FDG imaging can be used to differentiate between malignant tumors and inflammatory processes [9].

With specifically targeted radiotracers, such as 3-N-[11C]-methylspiperone which targets the dopamine D2 receptors in the basal ganglia [10], high spatial resolution imaging equipment is no longer needed. In such cases, a simple dual-probe coincidence detecting system is enough to provide information about the dynamic uptake of the tracer in the targeted organ [11,12]. In recent years, a high-throughput coincidence planar imaging device was desired for large-scale drug-screening using positron radiotracers [13,14]. Therefore, a coincidence detection device, the Institute of Nuclear Energy Research (INER) Animal Rotating Positron Emission Tomography (ARO-PET) scanner, was constructed to detect annihilation gamma rays using either rotating detectors for tomography imaging or fixed detectors for dynamic coincidence planar images [15].

In this study, we set up an experimental paradigm by determining [18F]FDG dynamic uptake in tumors and inflammations in nude mice models using the ARO-PET scanner to perform coincidence planar imaging as the foundation of future research applications. The possibility of differentiating between malignant tumors and inflammations was tested by comparing [18F]FDG uptake at different imaging time points. The distribution of [18F]FDG uptake in malignancy and inflammation in nude mice was also demonstrated by histopathology and micro-autoradiography.

Materials and Methods

System characteristics

The ARO-PET system was constructed and performance characteristics validated by the physics and instrument group at the INER [15]. It was constructed using four detectors in a rotating gantry. Each detector consists of an 18×16 array of bismuth germinate crystal and is coupled to a Hamamatsu R3941 position-sensitive photomultiplier tube. Each crystal is $2.6 \times 2.6 \times 25.0$ mm. Detector-to-detector distance can vary from 22 to 38 cm. The effective field of view is 5.0 cm (axial) $\times$ 4.4 cm (transaxial). The spatial resolution (full width at half maximum) of the system at the center is 2.73 mm [15]. In a previous study, we demonstrated that the ARO-PET scanner system can be used to acquire dynamic coincidence planar images without rotating the detectors [16].

Human cancer model and inflammations in nude mice

The study was performed according to the National Research Council's *Guide for the Care and Use of Laboratory Animals* and the recommendations of the committee on animal research at the INER [17]. The protocol was fully approved by the institutional review committee on animal care. Eight female nude mice (17–20 g, 4 weeks old) were purchased from the National Laboratory Animal Breeding and Research Center in Taipei, Taiwan. They were housed in sterile filter-top cages on sterile bedding, and were fed with an irradiated diet and autoclaved water.

To produce the cancer model, 1×10^6 cells in 0.1 mL of culture medium was injected subcutaneously into the right hind thighs of six nude mice, two with lung cancer cells, two with nasopharyngeal cancer cells, and two with thyroid cancer cells. The tumors were allowed to grow for 1–3 weeks to about 1 cm^3 in size.

To induce inflammations, 0.1 mL of turpentine oil was subcutaneously injected into the right hind thigh of one nude mouse for each day for 4 days and another nude mouse every day for 8 days before [18F]FDG dynamic study [18].

Dynamic [18F]FDG coincidence planar imaging

Prior to [18F]FDG imaging, animals had food withdrawn overnight. All animals were anesthetized with 65 mg/kg of sodium pentobarbital (MTC Animal Health, Cambridge, ON, Canada) given as an intraperitoneal injection. After anesthesia, each mouse was placed on the imaging table in the center of the field of view. The [18F]FDG, which was

synthesized and radiolabeled using automatic apparatus at INER, was injected through the tail veins.

Serial dynamic coincidence planar images were acquired immediately after injection of 0.6–0.7 mCi of [^{18}F]FDG. The ARO-PET scanner acquired images with a 35 × 31 matrix size for 4 hours, and the images were binned into a series of sequential 30-second frames. A time versus lesion-to-background ratio curve was generated by drawing regions of interest over the tumor or inflammation (lesion activity) and contralateral thigh (background activity). Equilibrium was defined when the lesion-to-background ratio [^{18}F]FDG reached a steady state. At equilibrium, 60 time points during a period 180–210 minutes after injection were chosen to calculate the mean equilibrium [^{18}F]FDG lesion-to-background ratio and the slope of the curves.

Histopathologic examination

Immediately after dynamic image acquisition, the mice were sacrificed for histopathologic examination. The tumors, inflammations, and contralateral thigh muscle were dissected. Tissue samples were embedded in an optimal cutting temperature compound (Miles Inc, Elkhart, IN, USA) and frozen in liquid nitrogen-cooled isopentane. The frozen samples were sectioned in a cryostat at –20°C. Contiguous 8 μm thick frozen sections were directly mounted on slides which were then stained with hematoxylin and eosin (H & E stain) for histopathologic examination.

In addition to H & E stain, nude mice with human thyroid cancer, nasopharyngeal cancer, and inflammations were also prepared for micro-autoradiography. The slides were coated with NTB2 nuclear emulsion (Eastman Kodak, Rochester, NY, USA) under a safety light and exposed in a light-proof box at 4°C. After exposure for 1 week, the emulsion slides were developed in 50% Kodak D19 (Eastman Kodak), fixed in polymax T fixer (Eastman Kodak), then stained with eosin Y (Shandom Inc, Pittsburgh, PA, USA). The silver grains in the micro-autoradiographs were examined under a light microscope.

Results

Dynamic [^{18}F]FDG coincidence planar imaging

The dynamic [^{18}F]FDG sequential planar projection images showed progressive accumulation of [^{18}F]FDG activity in the right hind thigh lesion as well as in the urinary bladder (Figure 1). The time versus lesion-to-background ratio curves of [^{18}F]FDG accumulations in tumors and inflammations showed a progressive increase in [^{18}F]FDG uptake pattern in the first 2 hours of the study and reached equilibrium approximately 3 hours after injection (Figure 2). In one of

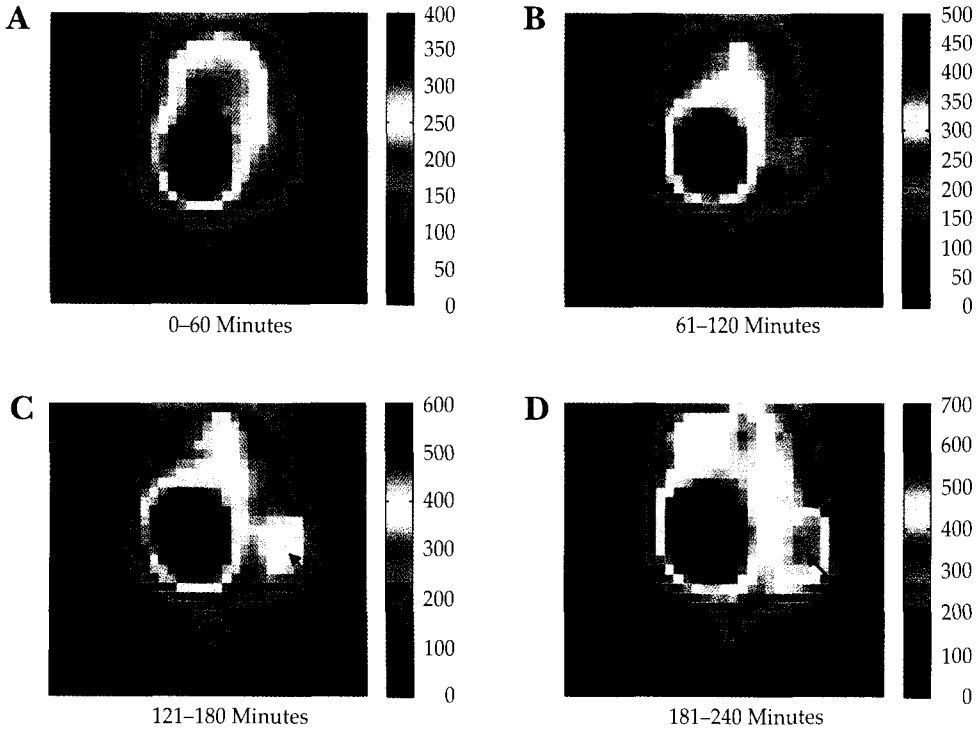

Figure 1. *Dynamic [^{18}F]FDG coincidence planar imaging of thyroid cancer-bearing nude mice after injection of radiotracer at: (A) 0–60 minutes; (B) 61–120 minutes; (C) 121–180 minutes; (D) 181–240 minutes. The images demonstrate progressive accumulation of [^{18}F]FDG in the tumor (arrow) as well as in the urinary bladder.*

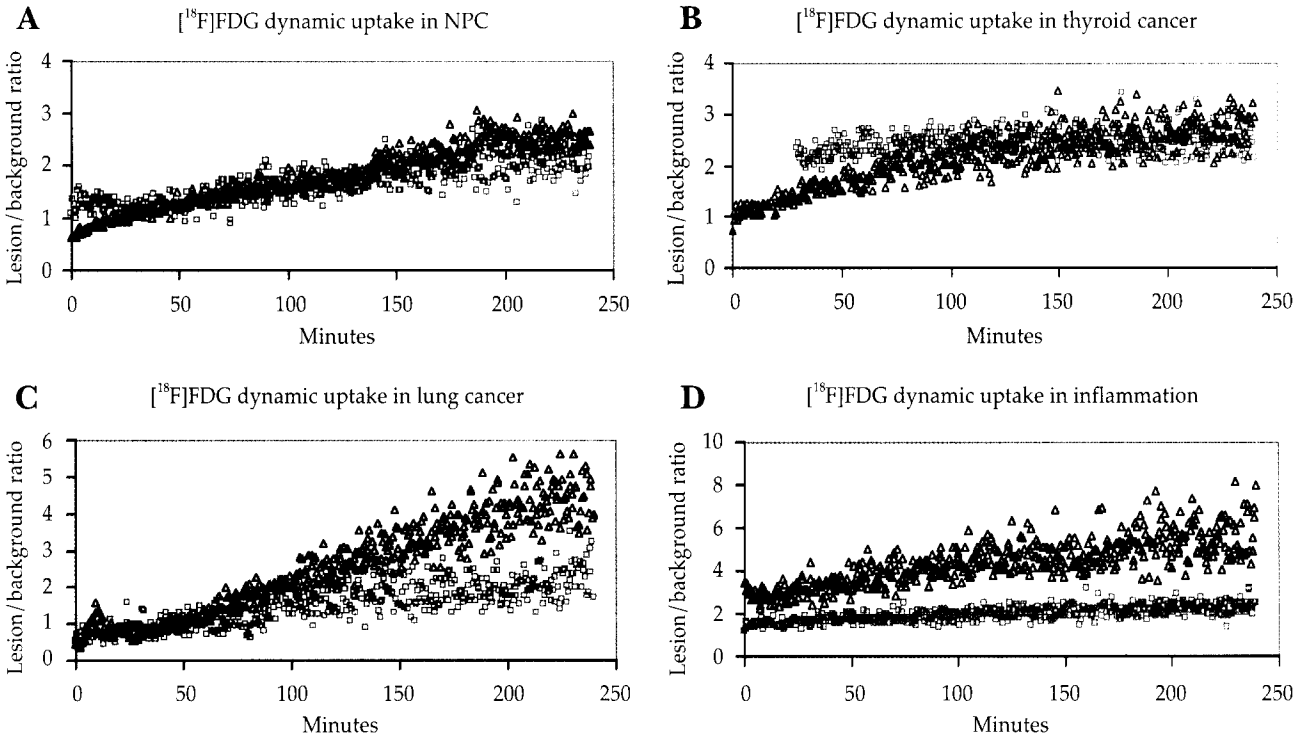

Figure 2. *Time–activity curves of [18F]FDG dynamic uptake in (A) nasopharyngeal cancer (NPC), (B) thyroid cancer, (C) lung cancer, and (D) turpentine-induced inflammations show progressively increased uptake of radioactivity in the first hour of the study. The lesion-to-background ratios reached equilibrium approximately 3 hours after injection. Pink squares and blue triangles represent the changes in lesion-to-background ratios in two mice corresponding to each data acquisition time point.*

the thyroid cancer-bearing mice, the first 30 minutes of data were lost due to technical problems.

The [18F]FDG lesion-to-background uptake ratios for the tumors and inflammations at equilibrium are listed in the Table. The slopes of the [18F]FDG time versus lesion-to-background ratio curves 180–210 minutes after injection are also listed. By definition, at equilibrium, the slopes changed very little.

Histopathologic examination and micro-autoradiography

Photomicrographs of turpentine-induced inflammations showed the abscess center, inner layer of inflammation cells, granulation tissue, and subcutaneous tissue (Figure 3A). The abscess center consisted of turpentine and cell debris. A large number of round and polymorphonuclear cells and exudates were observed in the inner layer of inflammatory cells (Figure 3B). The granulation tissue showed a mixed cellular infiltrate of polymorphonuclear cells, macrophages, and fibroblasts around the lesion. The micro-autoradiograph showed heavy grain density in the granulation tissue (Figures 3C and D). There was increased [18F]FDG uptake in the area with a high concentration of macrophage and polymorphonuclear cells.

Malignant tumors could also be divided into three distinct histologic areas: the tumor center, consisting of tumor cells and cell debris, and granulation and subcutaneous tissue (Figure 4A). In the granulation tissue,

Table. Means ± standard deviations of lesion-to-background ratios and slopes of the time versus lesion-to-background ratio curves for tumors and inflammations at equilibrium 180–210 minutes after [18F]FDG injection

	LTB ratio	Slope (/min)
NPC (1)	2.49 ± 0.24	0.00669
NPC (2)	2.06 ± 0.30	0.00085
Thyroid cancer (1)	2.61 ± 0.28	0.00429
Thyroid cancer (2)	2.46 ± 0.24	0.00368
Lung cancer (1)	4.04 ± 0.57	0.02055
Lung cancer (2)	1.97 ± 0.34	–0.00207
Inflammation (4-day)	2.26 ± 0.26	0.00642
Inflammation (8-day)	5.47 ± 0.90	0.00825

NPC = nasopharyngeal cancer; LTB = lesion-to-background.

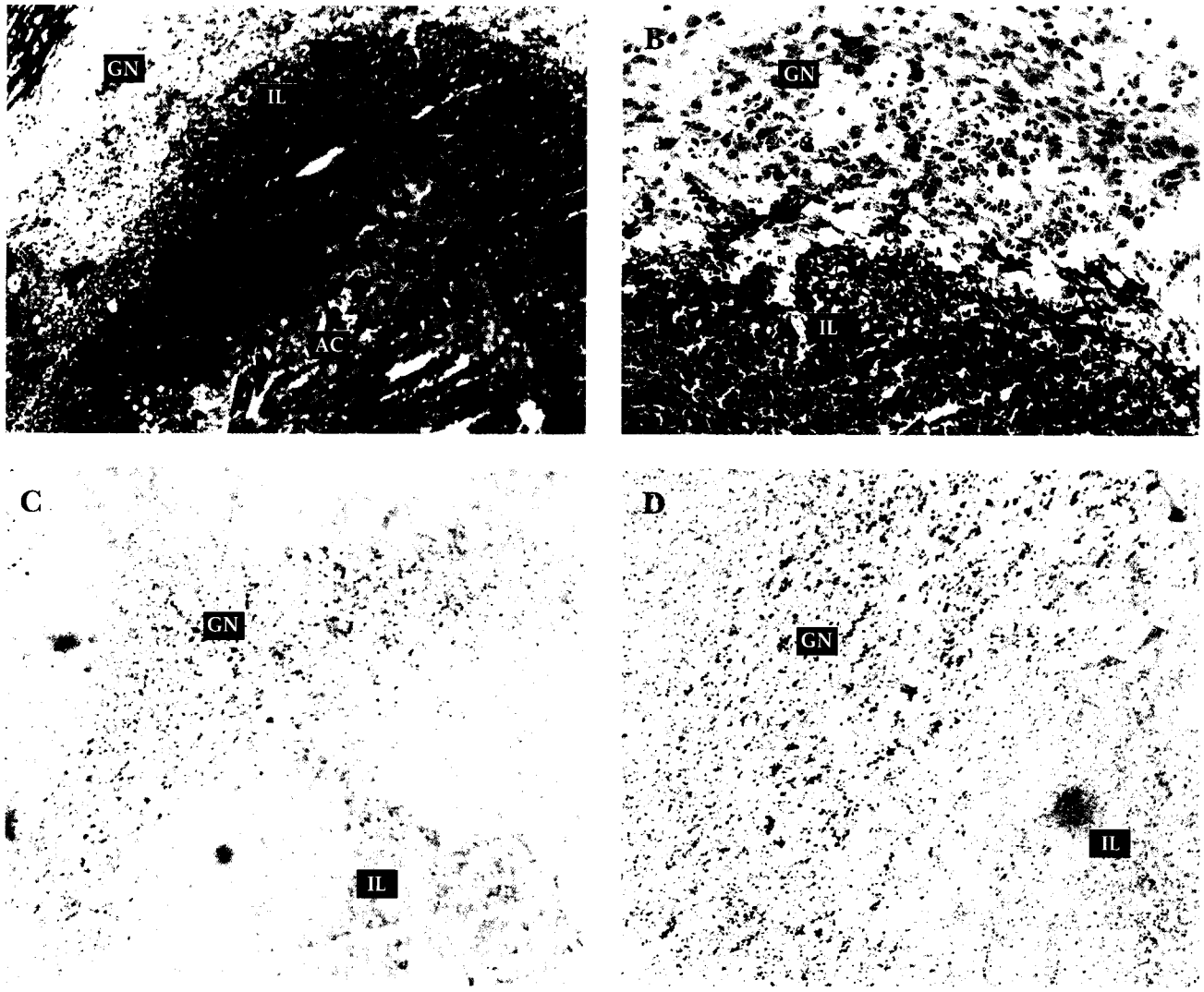

Figure 3. *Turpentine-induced inflammations: (A, B) histology samples stained with hematoxylin and eosin (×40 and ×100, respectively) and (C, D) micro-autoradiographs (×40 and ×100, respectively). The lesion is characterized by an abscess center (AC), inner layer (IL) of inflammatory cells mainly consisting of polymorphonuclear cells, and granulation tissue (GN). The granulation tissue consists of a mixed cellular pattern of polymorphonuclear cells, macrophages, and fibroblasts. The area with increased [^{18}F]FDG accumulation correlates with granulation tissue.*

fibroblasts and round phagocyte cells (macrophages and neutrophils) were present. The granulation tissue formed the wall of the tumor (Figure 4B). Micro-autoradiography of a thyroid cancer-bearing nude mouse showed heavy grain density in the granulation and tumor tissues (Figures 4C and D). The lowest grain density was in the thigh muscle (Figure 4E).

Discussion

In this study, a paradigm of dynamic [^{18}F]FDG uptake coincidence imaging was demonstrated. The tumors and inflammations in the right hind legs of nude mice were clearly seen in coincidence planar images (Figure 1). The [^{18}F]FDG time versus lesion-to-background ratio curves corresponded well with the dynamic coincidence planar images (Figure 2). Dynamic [^{18}F]FDG coincidence imaging can help in determining a suitable time point for microPET image acquisition in tumors and inflammations in nude mice models in future experiments.

[^{18}F]FDG is a useful tumor-detecting radiotracer. [^{18}F]FDG accumulation in the malignant tissue is due to the increase in glucose transporter expression and hexokinase activity and the decrease in glucose-6-phosphate phosphatase activity in malignant cells [19–22]. Inflamma-

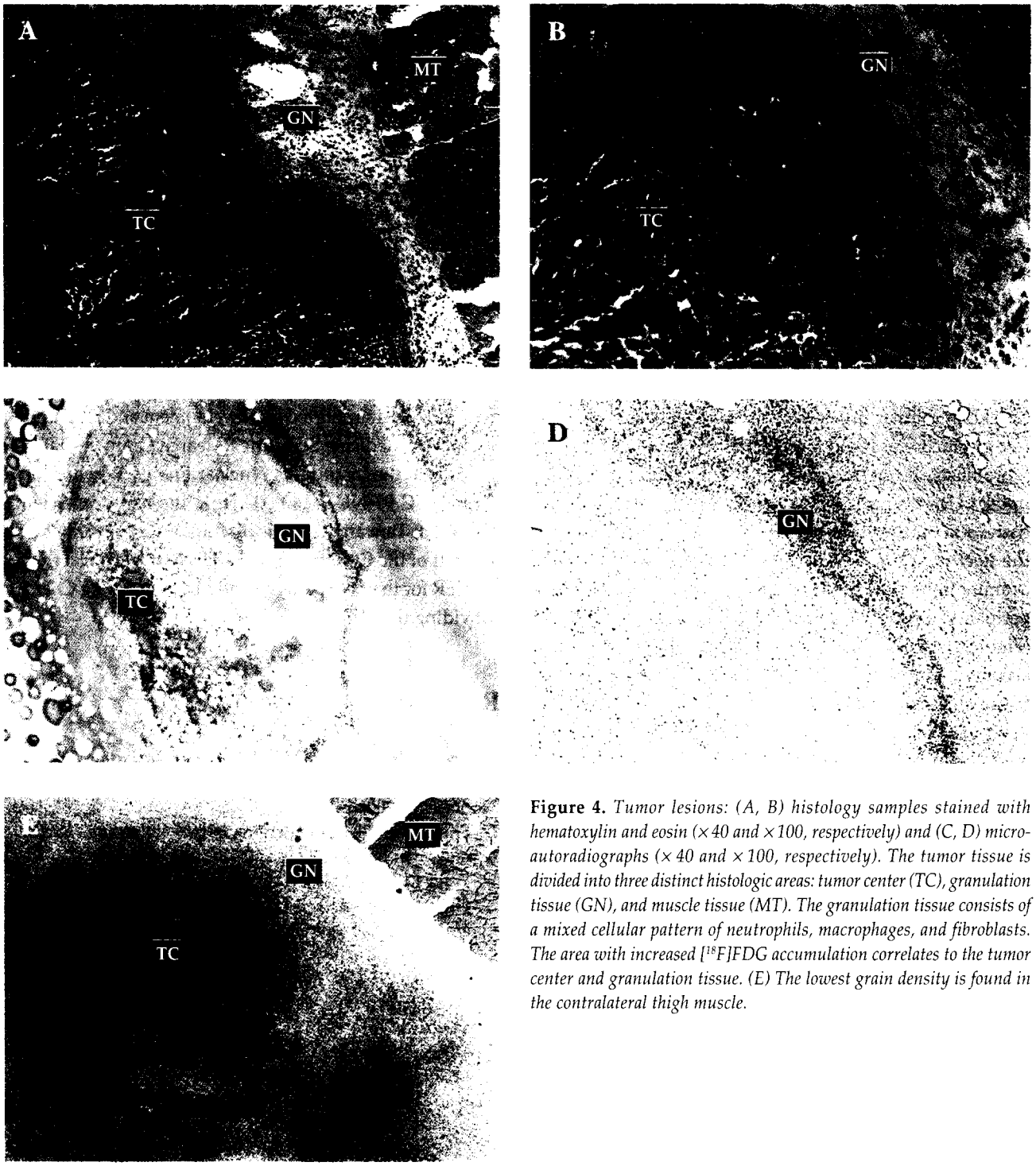

Figure 4. *Tumor lesions: (A, B) histology samples stained with hematoxylin and eosin (×40 and ×100, respectively) and (C, D) micro-autoradiographs (×40 and ×100, respectively). The tumor tissue is divided into three distinct histologic areas: tumor center (TC), granulation tissue (GN), and muscle tissue (MT). The granulation tissue consists of a mixed cellular pattern of neutrophils, macrophages, and fibroblasts. The area with increased [18F]FDG accumulation correlates to the tumor center and granulation tissue. (E) The lowest grain density is found in the contralateral thigh muscle.*

tory cells such as macrophages and neutrophils also exhibit increased [^{18}F]FDG uptake, which can be clearly visualized *in vivo* in sites of inflammation and infection [23]. Even though both tumors and inflammations accumulate [^{18}F]FDG, Zhuang et al reported that dual-time [^{18}F]FDG PET imaging can differentiate between malignant and inflammation processes [9]. Their time course study of [^{18}F]FDG tissue distribution showed that the uptake in inflammations increased gradually until 60 minutes and then decreased. However, this dynamic [^{18}F]FDG imaging study showed a progressive and consistent increase in [^{18}F]FDG lesion-to-background ratios in both malignant

tumors and turpentine-induced inflammations in nude mice. Dynamic uptake of [^{18}F]FDG into both tumors and inflammations reached equilibrium approximately 3 hours after injection.

In a [^{18}F]FDG micro-autoradiography study, Yamada et al demonstrated a high density of silver grains in an abscess wall consisting of an inflammatory cell layer and granulation tissue [18]. The highest grain density was found in the marginal zone of young fibroblasts, endothelial cells of vessels, and phagocytes of neutrophils and macrophages, followed by that in the neutrophil layer and granulation tissue. Kaim et al demonstrated the highest [^{18}F]FDG in areas of inflammatory cell infiltrates in experimental bacterial abscesses in rats [24]. The increasing [^{18}F]FDG uptake in cellular infiltrates with time suggests a higher rate of glucose usage in macrophages than in neutrophils. Fibroblasts did not substantially contribute to [^{18}F]FDG uptake. However, [^{18}F]FDG also accumulates in granulation tissue and macrophages infiltrating the areas surrounding the necrotic tumor tissue [24]. In this study, histologic examinations showed a layer of granulation tissue at the periphery of both malignant tumor and inflammation tissue (Figures 3A and 4A). Micro-autoradiography showed that accumulation of [^{18}F]FDG was higher in young granulation tissue and macrophages surrounding inflammations and malignant tumors (Figures 3C and 4C). This granulation tissue also contributes to the uptake of [^{18}F]FDG into inflammations and partially into malignant tumors. Kubota et al reported similar results, that newly formed granulation tissue around the tumor and macrophages take up more [^{18}F]FDG than viable tumor cells [25]. The [^{18}F]FDG uptake in inflammation may vary depending on the different phases of the inflammation process. Yamada et al reported that the maximum [^{18}F]FDG accumulation in turpentine-induced inflammation is observed in the chronic phase characterized histologically by chronic inflammation [18]. In this study, we also found that the mean lesion-to-background ratio of [^{18}F]FDG uptake was higher in the 8-day inflammation than the 4-day inflammation at equilibrium.

Kubota et al reported that [^{18}F]FDG uptake shows cell cycle dependency, with a higher uptake observed in cells in G0/G1 and G2 phases of the cell cycle compared with those in the S and M phases [25]. We believe that the different inoculation periods of tumor growth in this study may have influenced [^{18}F]FDG uptake. In addition, the different malignant tumor cell types may also have affected uptake. Therefore, it is essential to determine the characteristics of each cancer cell type in the nude mouse model before using [^{18}F]FDG animal PET as a tool for chemotherapy evaluation in new drug development.

These preliminary results suggested that dynamic [^{18}F]FDG coincidence planar imaging can help in determining a suitable time for static [^{18}F]FDG imaging in tumors and inflammations in nude mice models. In this study, the optimal time for static [^{18}F]FDG PET imaging at a good and steady lesion-to-background ratio was around 3 hours after injection. The study demonstrated a paradigm for nude mouse models in determining dynamic [^{18}F]FDG uptake pattern for future experiments.

Acknowledgments

This work was supported by Development and Application of Nuclear Medicine Scientific Research Grant 90-2001-14-05-05 from the Institute of Nuclear Energy Research, and Grant NSC 93-NU-7-182-002 from the National Science Council of Taiwan, Republic of China. We gratefully thank the staff of the Cyclotron and Radiopharmaceutical Center of INER for their cooperation and Mr. Jenn-Pzong Chen for providing the [^{18}F]FDG.

References

1. Phelps ME. History of PET. In: Delbeke D, Martin WH, Patton JA, et al, eds. *Practical FDG Imaging: A Teaching File*. New York: Springer, 2002:1–17.
2. Phelps ME. PET: the merging of biology and imaging into molecular imaging. *J Nucl Med* 2000;41:661–81.
3. Wahl RL. Principles of cancer imaging with fluorodeoxyglucose. In: Wahl RL, Buchanan JW, eds. *Principles and Practice of Positron Emission Tomography*. Philadelphia: Lippincott Williams and Wilkins, 2002:100–10.
4. Coleman RE. FDG imaging. *Nucl Med Biol* 2000;27:689–90.
5. Weber G. Enzymology of cancer cells. *N Engl J Med* 1977;296:541–51.
6. Higashi K, Clavo AC, Wahl RL. Does FDG uptake measure proliferative activity of human cancer cells? *In vitro* comparison with DNA flow cytometry and tritiated thymidine uptake. *J Nucl Med* 1993;34:414–9.
7. Coleman RE, Tesar R, Phelps M. HCFA and expanded coverage of PET. *J Nucl Med* 2001;42:11N–12N.
8. Zhao S, Kuge Y, Tsukamoto E, et al. Effects of insulin and glucose loading on FDG uptake in experimental malignant tumors and inflammatory lesions. *Eur J Nucl Med* 2001;28:730–5.
9. Zhuang H, Pourdehnad M, Lambright ES, et al. Dual time point [F-18] FDG PET imaging for differentiating malignant from inflammatory processes. *J Nucl Med* 2001;42:1412–7.
10. Wagner HN Jr, Burns HD, Dannals RF, et al. Imaging dopamine receptors in the human brain by positron tomography. *Science* 1983;221:1264–6.

11. Jeffries KJ, Kim S, Wagner HN Jr. *In vivo* probes: pharmacological studies. In: Wagner HN Jr, Szabo Z, Buchanan JW, eds. *Principles of Nuclear Medicine*, 2nd edition. Philadelphia: W.B. Saunders, 1995:175–85.
12. Kao PF, Huang JY, Wang CH, Tzen KY. Development of a dual-probe detection system for positron emission radiotracer detection. *Changgeng Yi Xue Za Zhi* 1998;21:139–45.
13. Siegel S, Vaquero JJ, Aloj L, et al. Initial results from a PET/Planar small animal imaging system. *IEEE Trans Nucl Sci* 1999; 46:571–5.
14. Green MV, Seidel J, Vaquero JJ, et al. High resolution PET, SPECT and projection imaging in small animals. *Comput Med Imaging Graph* 2001;25:79–86.
15. Jan ML, Liang HC, Huang SW, et al. The development of INER rotating positron emission tomography scanner for animal imaging. *Ann Nucl Med Sci* 2002;15:13–20. [In Chinese]
16. Sun YL, Jan ML, Kao PF, et al. Dynamic accumulation and distribution of [^{18}F]FDG in human thyroid cancer model on nude mice: by INER animal rotating PET scanner and microautoradiography. *Ann Nucl Med Sci* 2002;15:21–6.
17. Institute of Laboratory Animal Resources Commission on Life Sciences. *Guide for the Care and Use of Laboratory Animals*. Washington, DC: National Academy Press, 1996.
18. Yamada S, Kubota K, Kubota R, et al. High accumulation of fluorine-18-fluorodeoxyglucose in turpentine-induced inflammatory tissue. *J Nucl Med* 1995;36:1301–6.
19. Bomanji TB, Costa DC, Ell PJ. Clinical role of positron emission tomography in oncology. *Lancet Oncol* 2001;3:157–64.
20. Anderson H, Price P. What does positron emission tomography offer oncology? *Eur J Cancer* 2000;36:2028–35.
21. Waki A, Fujibayashi Y, Yokoyama A. Recent advances in the analyses of the characteristics of tumor on FDG uptake. *Nucl Med Biol* 1998;25:589–92.
22. Pauwels EK, Ribeiro MJ, Stoot JH, et al. FDG accumulation and tumor biology. *J Med Biol* 1998;25:317–22.
23. Kubota R, Yamada S, Kubota K, et al. Intratumoral distribution of fluorine-18-fluorodeoxyglucose *in vivo*: high accumulation in macrophages and granulation tissues studied by microautoradiography. *J Nucl Med* 1992;33:1972–80.
24. Kaim AH, Weber B, Kurrer MO, et al. Autoradiographic quantification of ^{18}F-FDG uptake in experimental soft-tissue abscesses in rats. *Radiology* 2002;223:446–51.
25. Kubota R, Kubota K, Yamada S, et al. Active and passive mechanisms of [fluorine-18] fluorodeoxyglucose uptake by proliferating and prenecrotic cancer cells *in vivo*: a microautoradiographic study. *J Nucl Med* 1994;35:1067–75.

裸鼠腫瘤及發炎模式之動態[氟-18]去氧葡萄糖攝取符時平面造影—組織病理學及微放射自動顯像術之相關對照研究

孫英玲[1] 詹美齡[1] 高潘福[2] 范國賢[1] 許惠婷[2] 張文震[3] 沈永吉[3] 李德偉[1]
[1]原子能委員會 核能研究所 [2]佛教新店慈濟綜合醫院暨慈濟技術學院 核子醫學科
[3]林口長庚紀念醫院 血液腫瘤科

核能研究所自行研發一部符時偵測儀，可用以進行小鼠正子放射製劑造影之研究，本實驗應用該符時偵測儀進行裸鼠腫瘤及發炎模式的 [氟-18] 去氧葡萄糖 (FDG) 藥物動力學研究，以動態連續造影方法觀察 FDG 在病灶處的攝取模式，以作為研發或測試治療癌症及發炎新藥的研究基礎。應用 6 隻腫瘤及 2 隻發炎模式裸鼠，在接受 25.9 百萬貝克 (MBq) 的 FDG 靜脈注射後進行連續 4 小時的動態攝影。資料經影像處理後，分別圈選病灶及對側大腿以作為計算病灶與背景放射活性的比值，當比值達到穩定時即定義為平衡狀態。所有裸鼠的病灶均接受組織學切片檢查，有 6 隻裸鼠的病灶並進行微放射自動顯像術檢查。在藥物動力學方面，FDG 在腫瘤及發炎病灶都在注射後三小時達到平衡狀態。腫瘤與背景放射活性的比值在 2.0–4.0 之間，發炎病灶在第四天及第八天的病灶與背景放射活性的比值分別為 2.3 及 5.5。組織學切片顯示巨噬細胞及中性白血球在腫瘤周圍及發炎病灶浸潤現象。顯微自動放射顯像術顯示有明顯銀染沉積現象。本研究顯示應用符時偵測儀可以決定裸鼠腫瘤及發炎模式的 FDG 最適切造影時間為靜脈注射後 3 小時。本研究映證應用動態連續造影方法可觀察未來新治療藥物處理後的 FDG 攝取變化的追蹤反應。

關鍵詞：[氟-18]去氧葡萄糖，裸鼠，動態符時平面造影

（高雄醫誌 2005;21:258–66）

收文日期：94 年 2 月 4 日
接受刊載：94 年 4 月 12 日
通訊作者：高潘福醫師
佛教新店慈濟綜合醫院核子醫學科
231 台北縣新店市建國路 289 號